Information Processing Letters 116 (2016) 373–378

Contents lists available at ScienceDirect

Information Processing Letters

www.elsevier.com/locate/ipl

Robust edge detector based on anisotropic diffusion-driven process

Baraka Jacob Maiseli [a,*], Huijun Gao [b]

[a] University of Dar es Salaam, College of Information & Communication Technologies, Department of Electronics & Telecommunication Engineering, P.O. Box 35194, Dar es Salaam, Tanzania
[b] Research Institute of Intelligent Control and Systems, Harbin Institute of Technology, Harbin, 150001, PR China

ARTICLE INFO

Article history:
Received 25 December 2014
Received in revised form 16 October 2015
Accepted 9 December 2015
Available online 15 December 2015
Communicated by X. Wu

Keywords:
Edge detector
Perona–Malik
Object detection
Image restoration
Information retrieval

ABSTRACT

Edge detection involves a process to discriminate, highlight, and extract useful image features (edges and contours). In many situations, we prefer an edge detector that distinguishes these features more accurately, and which comfortably deals with a variety of data. Our observations, however, discovered that most edge-defining functionals underperform and generate false edges under poor imaging conditions. Therefore, the current research proposes a robust diffusion-driven edge detector for seriously degraded images. The method is iterative, and suppresses noise while simultaneously marking real edges and deemphasizing false edges. The anisotropic nature of the new functional helps to remove noise and to preserve semantic structures. Even more importantly, the functional exhibits a forward–backward behavior that may sharpen and strengthen edges. Comparisons with some other classical approaches demonstrate superiority of the proposed approach.

1. Introduction

Edges in an image are regions with rapidly changing intensity values. Extracting these critical features forms an important step in many computer vision applications, such as industrial automation and control, and has been an interesting and challenging research question for years [1–4].

Humans are naturally equipped with senses to read, understand, and distinguish regions in the image (edges, contours, and flats). This is, however, a non-straightforward task for machines. Most machine-steered classical edge detectors underperform when input images are noisy, highly textured, or contain weak edges [3,5–7]. We should note that real-world scenes usually suffer from noise and other unwanted artifacts, thus prompting for robust and more effective segmentation methods to extract meaningful features.

In this letter, we propose an alternative edge detection approach based on anisotropic diffusion processes. The new method is iterative, and includes a robust feature-sensitive edge detector. In flat regions, the formulation follows isotropic diffusion that suppresses noise; and near edges, the detector gradually declines smoothing and highlights semantic features. The process is iterative and automatic, which helps the model to efficiently and robustly capture true edges in worse imaging conditions. The intriguing property of the proposed edge detector, which differentiates it from some other classical methods, is its ability to treat severely degraded scenes and reject false edges. The new algorithm is simple and contains repetitive operators that can promote parallel computing in a real hardware.

* Corresponding author.
E-mail address: barakamaiseli@yahoo.com (B.J. Maiseli).

http://dx.doi.org/10.1016/j.ipl.2015.12.003

2. Proposed diffusion-driven edge detector

Detecting edges and contours is perhaps the most critical step in almost all computer vision tasks. Before interpreting and analyzing real objects, machines need to precisely locate and register details of important features. To this end, several edge detectors have been proposed in the literature, with the classical ones being Canny, Sobel, Prewitt, and LoG (Laplacian of Gaussian). Despite their convincing performance, we noted from experimental results that the methods collapse for noisy input scenes.

In recent years, diffusion-based and total variation (TV) approaches have been widely applied to locate potential image features. Perona and Malik proposed a feature-dependent diffusivity (edge detector) [8], but scholars have proved that the Perona–Malik (PM) model suffers for staircasing problems and its corresponding energy potential is non-convex—thus prone to instabilities and multiple solutions [9,10]. Charbonnier et al. proposed an edge detector with a corresponding convex potential [11]. The weakness of Charbonnier's edge-defining functional is the unusual artifacts it produces in the restored scenes [12]. Weickert et al. established a nonlinear diffusion-driven edge detector, which is reliable and computationally inexpensive [13,14]. The authors applied a semi-implicit scheme (Additive Operator Splitting or AOS) to implement their method. For severely degraded images, however, Weickert's method fails to effectively capture potential features, thus limiting its applications. Rudin et al. provided an approach that uses total variation of an image to guide the diffusion process with diffusivity that is simply the reciprocal of the image gradient [15,16]. This diffusivity restores visually appealing edge maps (stronger and sharper). The weaknesses of TV-based edge detectors are blocking and staircasing artifacts [17,18].

Inspired by the weaknesses of the mentioned traditional approaches, we propose an alternative diffusion method that incorporates an edge-sensitive detector. In particular, the new edge detector is

$$\phi(|\nabla u|) = \frac{1+\frac{|\nabla u|}{K}}{1+\left(\frac{|\nabla u|}{K}\right)^2}, \tag{1}$$

where $K > 0$ is a tuning constant; ϕ divides the image domain, Ω, into two sub-domains: Ω_1, flat regions ($|\nabla u| \to 0$, $\phi \to 1$); and Ω_2, edges ($|\nabla u| \to \infty$, $\phi \to 0$). Plugging (1) into the general diffusion equation, we get the evolution equation

$$\frac{\partial u}{\partial t} = \operatorname{div}\left(\frac{1+\frac{|\nabla u|}{K}}{1+\left(\frac{|\nabla u|}{K}\right)^2}\nabla u\right) + \lambda(u-u_o), \tag{2}$$

where λ is a regularization parameter that establishes a trade-off between denoising and original images; u_o is the original image. To comprehensively understand the mechanics of (2) in the aspect of preserving image details, we further decompose it into tangential and normal components to the isophote lines, respectively denoted by u_{TT} and u_{NN}. Note that u_{TT} propagates along the contours and, thus, is responsible to protect edges. Our desire is to achieve a proper balance between u_{TT} and u_{NN}. Now, consider an arbitrary point (x, y) in the image, and orthogonal vectors, $T(x, y) = (u_x, u_y)/|\nabla u|$ and $N(x, y) = (-u_y, u_x)/|\nabla u|$ (inner product between T and N is zero or $< T, N >= 0$). Defining $u_{TT} = T'\nabla^2 uT$ and $u_{NN} = N'\nabla^2 uN$, equation (2) can compactly be written as

$$\frac{\partial u}{\partial t} = \left(\frac{1+\frac{|\nabla u|}{K}}{1+\left(\frac{|\nabla u|}{K}\right)^2}\right)u_{TT} + \left(\frac{1+2\frac{|\nabla u|}{K} - \left(\frac{\nabla u}{K}\right)^2}{\left(1+\left(\frac{|\nabla u|}{K}\right)^2\right)^2}\right)u_{NN} + \lambda(u-u_o). \tag{3}$$

In (3), homogeneous regions ($|\nabla u| \to 0$) receive linear isotropic diffusion ($\partial_t u = u_{TT} + u_{NN} + \lambda(u-u_o)$) that efficiently removes noise; and near boundaries ($|\nabla u| \to \infty$) u_{NN} is weaker because its coefficient diminishes faster, and u_{TT} dominates—a necessary condition to preserve edges. Our model has another important property that it may introduce backward diffusion, which sharpens edges [10,19], in locations where

$$\frac{|\nabla u|}{K} > 1+\sqrt{2}. \tag{4}$$

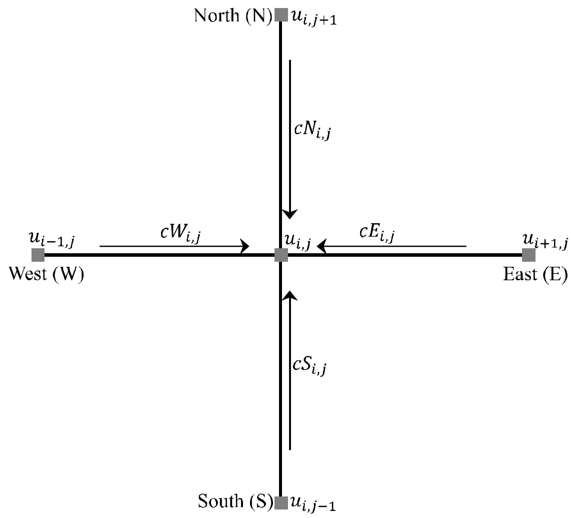

Fig. 1. Explicit numerical scheme.

3. Numerical implementation

We used a four-point neighborhood explicit scheme (Fig. 1) to implement our model. Unlike implicit schemes like adaptive operator splitting, which include relatively harder implementation strategies, explicit schemes are simpler, computationally efficient, and stable under Courant–Friedrichs–Lewy criterion ($0 < \tau \leq 0.25$; τ is the iteration step) [20].

Now, let us define gradients in the four directions of the scheme—North, South, East, and West—respectively as $\Delta^N_{i,j} = u_{i,j+1} - u_{i,j}$, $\Delta^S_{i,j} = u_{i,j-1} - u_{i,j}$, $\Delta^E_{i,j} = u_{i+1,j} - u_{i,j}$, and $\Delta^W_{i,j} = u_{i-1,j} - u_{i,j}$, and corresponding conduction coefficients as

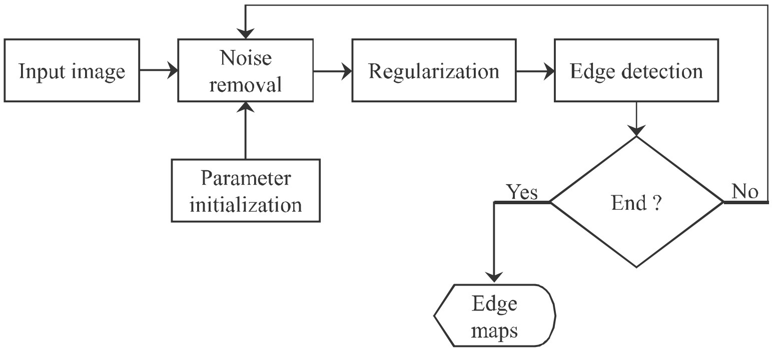

Fig. 2. Flow diagram of the proposed method.

$$cN_{i,j} = \frac{1+\frac{|\Delta^N_{i,j}|}{K}}{1+\left(\frac{|\Delta^N_{i,j}|}{K}\right)^2},\ cS_{i,j} = \frac{1+\frac{|\Delta^S_{i,j}|}{K}}{1+\left(\frac{|\Delta^S_{i,j}|}{K}\right)^2},$$

$$cE_{i,j} = \frac{1+\frac{|\Delta^E_{i,j}|}{K}}{1+\left(\frac{|\Delta^E_{i,j}|}{K}\right)^2},\ \text{and}\ cW_{i,j} = \frac{1+\frac{|\Delta^W_{i,j}|}{K}}{1+\left(\frac{|\Delta^W_{i,j}|}{K}\right)^2}.$$

The discretized divergence term is thus

$$\mathrm{div}_{i,j} = cN_{i,j}\Delta^N_{i,j} + cS_{i,j}\Delta^S_{i,j} + cE_{i,j}\Delta^E_{i,j} + cW_{i,j}\Delta^W_{i,j},$$

and steepest descent implementation that iteratively minimizes our objective function is

$$u^{(n+1)}_{i,j} = u^{(n)}_{i,j} + \tau(\mathrm{div}^{(n)}_{i,j} - \lambda(u^{(n)}_{i,j} - (u_o)_{i,j})). \quad (5)$$

And edge maps are built up in every iteration as

$$\phi^{(n+1)}_{i,j} = \phi^{(n)}_{i,j} + \frac{1+\frac{|\nabla u^{(n)}_{i,j}|}{K}}{1+\left(\frac{|\nabla u^{(n)}_{i,j}|}{K}\right)^2}. \quad (6)$$

Fig. 2 depicts the implementation diagram of the new model.

A critical and challenging task in iterative methods, like ours, is to establish a stopping mechanism. In this letter, we have developed a new strategy to stop iterations that uses peak-signal-to-noise-ratio (PSNR) [21] or mean-structural-similarity (MSSIM) [22]. We discovered that as an image evolves the curves for PSNR and MSSIM become concave, and the maximum point of either curve signals an optimal image and can, therefore, help to designate an exit condition (Fig. 3). Assuming PSNR is used as a stopping condition: let $L^{n-1}_{\max}$ be the maximum PSNR, and L^n and L^{n-2} be the PSNR in the neighborhood of $L^{n-1}_{\max}$; optimal conditions are achieved when $(L^{n-1}_{\max} - L^{n-2}) \times (L^n - L^{n-1}_{\max}) \leq 0$. Note that this technique works well in a simulation environment where the original image is known.

4. Results

Visual results show that when images are heavily corrupted by noise, most old edge detectors—particularly Canny, LoG, TV, and PM—generate false and/or weaker

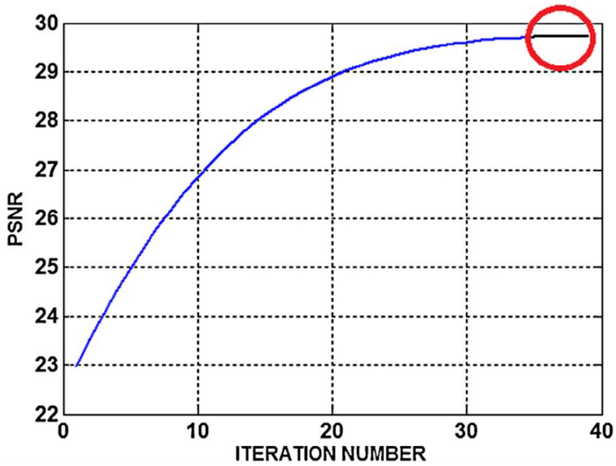

Fig. 3. Stopping mechanism.

edges. Our method, however, produces well-defined and stronger edges and efficiently suppresses unwanted artifacts (Figs. 4–6). These observations can be objectively quantified in Tables 1 and 2, where our method yields higher quality values.

5. Discussions

We quantified our results using an edge-similarity-metric (ESIM) in [23,24], which addresses potential weaknesses of traditional quality metrics (which is that they fail to measure the strength and quality of edges). The ESIM is defined by

$$\mathrm{ESIM} = \widetilde{\mathrm{PSNR}}(\mathrm{EM}(u), \mathrm{EM}(u_o)), \quad (7)$$

where $\mathrm{EM}(u)$ and $\mathrm{EM}(u_o)$ are, respectively, the edge maps of u (processed image) and u_o (original image), and

$$\widetilde{\mathrm{PSNR}} = 10\log_{10}\frac{PQ\,|\max(u_o) - \min(u_o)|^2}{\|u - u_o\|_2^2}$$

is as defined in [24]; P and Q are horizontal and vertical runs of either u or u_o, respectively. An image with several false edges possesses lower value of ESIM. Also, stronger and well-distinguished edges raise the value of ESIM.

Tables 1 and 2 demonstrate that the proposed edge detector is superior as it provides higher values of ESIM. The ability of our edge detector to robustly identify and

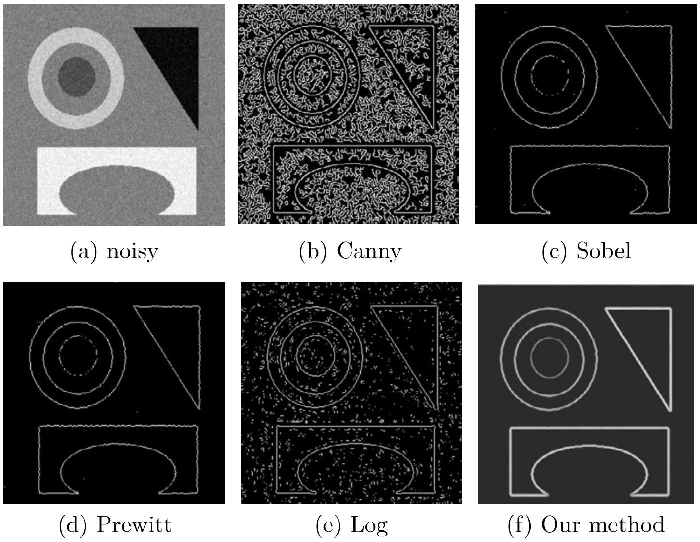

Fig. 4. Gradient-driven edge detectors versus our method (noise is additive of standard deviation 20).

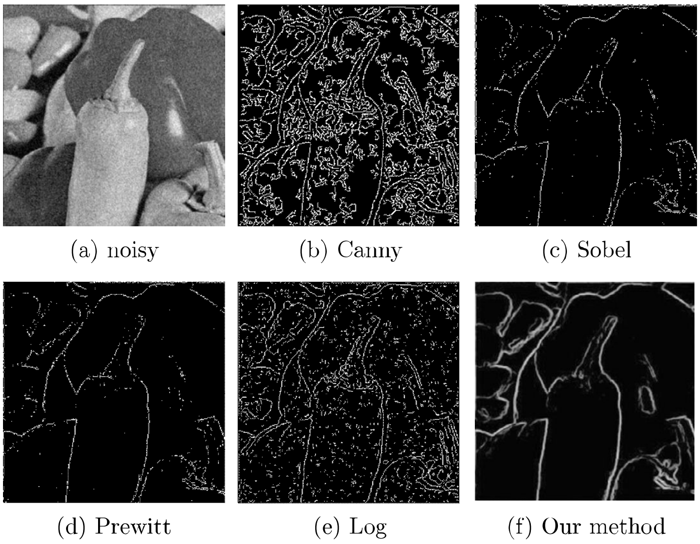

Fig. 5. Gradient-driven edge detectors versus our method (noise is additive of standard deviation 20).

highlight edges of noisy images is caused by nonlinear properties of the well-crafted diffusion coefficient in (1)—uniform smoothing in flat regions, which removes noise; and anisotropic smoothing near edges, which preserves edges. Furthermore, the new method extracts natural edges, then sharpens and strengthens them as it possesses a backward-diffusion behavior, as equation (4) depicts.

Additionally, the iterative process of the proposed method converges faster and is stable because of its well-behaved convexity property. To prove this, the energy functional, $\rho(s)$, from (2) is first derived. Thus, we solve the problem

$$\rho(s) = \int_{\Omega} \frac{(1+s)s}{1+s^2}\,\mathrm{d}\Omega, \tag{8}$$

where $s = \frac{|\nabla u|}{K}$, and get $\rho(s) = \frac{1}{2}\ln(1+s^2) + s - \arctan(s)$. For $K > \frac{s}{1+\sqrt{2}}$, $\rho(s)$ is strictly convex because $\rho''(s) = \frac{1+2s-s^2}{(1+s^2)^2} > 0$.

The major limitation of our method is that the parameter K, which controls smoothness and clarity of edges, is manually chosen. The method may generate undesirable results if K is inappropriate. In the future, we intend to address the issue by developing an automatic mechanism to select K.

6. Conclusion

This paper has proposed a diffusion-driven iterative method to extract edges from noisy images. Both qualitative and quantitative results demonstrate the effectiveness of the method to generate stronger and clearer edges. As the new approach is robust against noise, it can benefit most computer vision tasks for real world scenes.

The next phase of the research is to use the proposed diffusion equation in (2) as a regularizer to address the ill-posedness of some inverse problems. In particular, we shall start with the super-resolution image reconstruction problem [25]; that is, solving the minimization problem

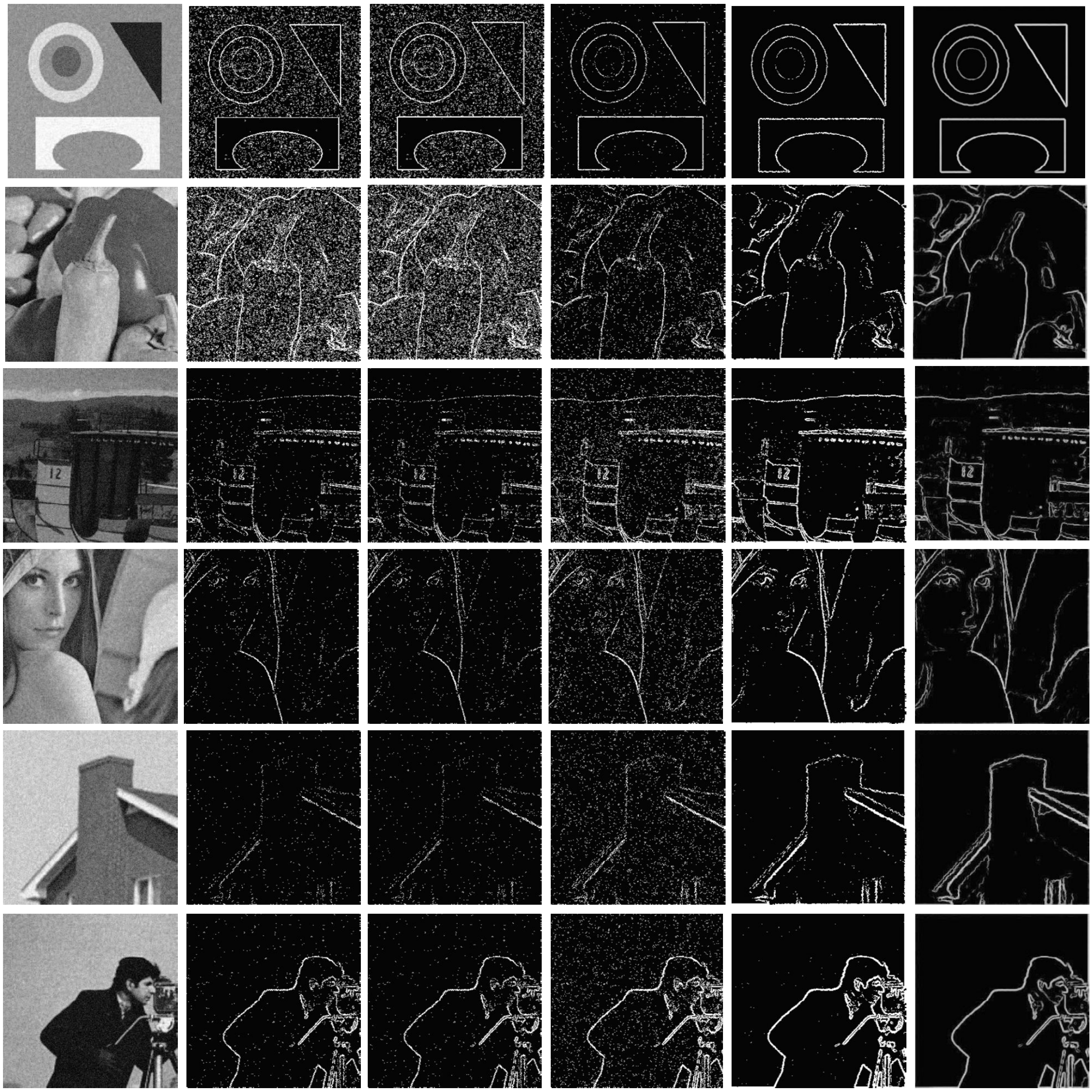

(a) noisy (b) TV (c) PM (d) Weickert (e) Guo (f) Ours

Fig. 6. Diffusion-driven edge detectors versus our method (noise is additive of standard deviation 20).

Table 1
Edge similarity strength (ESIM) measurements of gradient-driven edge detectors.

Image	ESIM				
	Canny	Sobel	Prewitt	LoG	Ours
Synthetic	6.41	16.62	16.62	12.20	20.73
Natural	8.57	11.54	11.55	9.71	12.70

$$\min_u \left\{ \frac{1}{2M} \sum_{k=1}^{M} \|y_k - T_k u\|^2_{L^2(\Omega)} + \|\rho(|\nabla u|)\|_{L^1(\Omega)} \right\}, \quad (9)$$

where: T_k, degradation (transformation) matrix; and M, number of degraded frames.

Table 2
Edge-similarity-strength (ESIM) measurements of diffusion-driven edge detectors.

Image	ESIM				
	TV	PM	Weickert	Guo	Ours
Contours	5.22	11.33	13.98	12.20	18.01
Peppers	4.73	5.51	6.50	8.09	16.33
Journey	6.42	5.70	5.13	10.12	16.84
Lena	4.20	4.17	4.15	9.93	15.89
House	4.01	4.01	4.00	8.11	10.34
Cameraman	7.12	11.07	12.10	11.95	17.23

Acknowledgement

The authors of this manuscript declare that none of the organizations funded the research.

References

[1] J. He, L. Hou, W. Zhang, A kind of fast image edge detection algorithm based on dynamic threshold value [j], Sens. Transducers 24 (2013) 179–183.

[2] S.S. Al-Amri, N. Kalyankar, S. Khamitkar, Image segmentation by using edge detection, Int. J. Comput. Sci. Eng. 2 (2010) 804–807.

[3] W. Gao, X. Zhang, L. Yang, H. Liu, An improved Sobel edge detection, in: 3rd IEEE International Conference on Computer Science and Information Technology, ICCSIT, vol. 5, IEEE, 2010, pp. 67–71.

[4] R. Biswas, J. Sil, An improved canny edge detection algorithm based on type-2 fuzzy sets, Proc. Technol. 4 (2012) 820–824.

[5] W. McIlhagga, The canny edge detector revisited, Int. J. Comput. Vis. 91 (2011) 251–261.

[6] K. Yu, Z. Xie, A fusion edge detection method based on improved Prewitt operator and wavelet transform, Engineering Technology and Applications, 2014, p. 289.

[7] K.J. Karande, S.N. Talbar, Laplacian of Gaussian edge detection for face recognition using ICA, in: Independent Component Analysis of Edge Information for Face Recognition, Springer, 2014, pp. 35–47.

[8] P. Perona, J. Malik, Scale-space and edge detection using anisotropic diffusion, IEEE Trans. Pattern Anal. Mach. Intell. 12 (1990) 629–639.

[9] S. Kichenassamy, The Perona–Malik paradox, SIAM J. Appl. Math. 57 (1997) 1328–1342.

[10] P. Guidotti, A backward–forward regularization of the Perona–Malik equation, J. Differ. Equ. 252 (2012) 3226–3244.

[11] P. Charbonnier, L. Blanc-Feraud, G. Aubert, M. Barlaud, Two deterministic half-quadratic regularization algorithms for computed imaging, in: Image Processing, 1994. Proceedings, ICIP-94, IEEE International Conference, vol. 2, 1994, pp. 168–172.

[12] B.J. Maiseli, Q. Liu, O.A. Elisha, H. Gao, Adaptive Charbonnier super-resolution method with robust edge preservation capabilities, J. Electron. Imaging 22 (2013) 043027.

[13] J. Weickert, B.T.H. Romeny, M. Viergever, et al., Efficient and reliable schemes for nonlinear diffusion filtering, IEEE Trans. Image Process. 7 (1998) 398–410.

[14] J. Weickert, Theoretical Foundations of Anisotropic Diffusion in Image Processing, Springer, 1996.

[15] L.I. Rudin, S. Osher, E. Fatemi, Nonlinear total variation based noise removal algorithms, Phys. D, Nonlinear Phenom. 60 (1992) 259–268.

[16] P. Getreuer, Rudin–Osher–Fatemi total variation denoising using split Bregman, Image Process. Line 10 (2012).

[17] B. Wu, E.A. Ogada, J. Sun, Z. Guo, A total variation model based on the strictly convex modification for image denoising, Abstr. Appl. Anal. 2014 (2014), Hindawi Publishing Corporation.

[18] E.A. Ogada, Z. Guo, B. Wu, An alternative variational framework for image denoising, Abstr. Appl. Anal. 2014 (2014), Hindawi Publishing Corporation.

[19] P. Lafitte, C. Mascia, Numerical exploration of a forward–backward diffusion equation, Math. Models Methods Appl. Sci. 22 (2012).

[20] R. Courant, K. Friedrichs, H. Lewy, On the partial difference equations of mathematical physics, IBM J. Res. Dev. 11 (1967) 215–234.

[21] Z. Wang, A.C. Bovik, Mean squared error: love it or leave it? A new look at signal fidelity measures, IEEE Signal Process. Mag. 26 (2009) 98–117.

[22] Z. Wang, A.C. Bovik, H.R. Sheikh, E.P. Simoncelli, Image quality assessment: from error visibility to structural similarity, IEEE Trans. Image Process. 13 (2004) 600–612.

[23] Z. Guo, J. Sun, D. Zhang, B. Wu, Adaptive Perona–Malik model based on the variable exponent for image denoising, IEEE Trans. Image Process. 21 (2012) 958–967.

[24] S. Durand, J. Fadili, M. Nikolova, Multiplicative noise removal using L1 fidelity on frame coefficients, J. Math. Imaging Vis. 36 (2010) 201–226.

[25] X. Zeng, L. Yang, A robust multiframe super-resolution algorithm based on half-quadratic estimation with modified BTV regularization, Digit. Signal Process. 23 (2013) 98–109.